Geomagnetic field measurements: instrument calibration and data processing

Author: Helena Bermúdez González, hbermugo7@alumnes.ub.edu
Facultat de Física, Universitat de Barcelona, Diagonal 645, 08028 Barcelona, Spain.

Advisor: Anna Martí Castells, annamarti@ub.edu

Abstract: In the field of geophysics, the time variations in the electric and magnetic fields are used to study solar activity and the geomagnetic field, and to characterise the electrical properties of the subsurface. It is important to know the operational range and limitations of the sensors and the data logger used for the data digitalization. Time series processing allows converting the recorded signals to the frequency and to calculate the transfer functions. The objective of this work is to compare the time series and geomagnetic transfer functions obtained with two different instruments and with the ones obtained using data from the Ebre Observatory. As the data were registered at similar latitudes as the observatory, a comparison can be conducted with integrity. The results show some similarities and discrepancies between both the time signals and the transfer functions. It is also notable that none of the tested instruments performed better than the other in the collective outcome.
Keywords: Geomagnetic field, Maxwell's equations, tipper, time series analysis, magnetotelluric method.
SDGs: This work can be related with ODS's 7 and 9.

I. INTRODUCTION

In geophysics, applied geophysics is the branch that involves the study of the subsurface using different techniques. One of these techniques is the magnetotelluric method (MT), which is based on the measurement of natural electromagnetic field variations. The transfer functions (TFs), which characterize the electrical conductivity of the subsurface, can be obtained from the relationships between the recorded fields in the frequency domain [1]. Among the TFs, the relation between the vertical and horizontal components of the geomagnetic field is referred to as the geomagnetic TF or tipper. For the measurement of the magnetic field, induction coils or flux magnetometers can be used, depending on the working frequency range. In this work, flux-gate magnetometers will be considered.

This study involves the setup and calibration of two different instruments consisting of a three-axis fluxgate magnetometer and a data logger. One instrument, referred to as Bartington, is composed of a Bartington magnetometer Mag-03MS70, and a DigOS data logger DATA-CUBE3. The second instrument, referred to as Lemi, is from LEMI LLC and consists of a magnetometer with its own data logger. The magnetic field is simultaneously measured using the two stations at the same location, near Rofes, and analysed with a custom-build program developed for this study. A comparative study of the time series and the TF derived from each station is then conducted.

Magnetic field data recorded on the same day by the Ebre Observatory [2] with another LEMI is also analysed and compared to the data recorded in Rofes. Although the 150 km distance, thus the slight latitude difference, will cause differences on the time series and TFs due to local effects (conductive anomalies in the subsurface), the carefully calibrated and isolated instruments from the Ebre provide a reliable source of data for comparing the behaviour of the Rofes results.

II. THE FLUX-GATE MAGNETOMETER

As detailed in [3], the flux-gate magnetometer is a vector magnetometer, as it measures the magnitude of the magnetic field at a particular direction. Its functionality is based on the principle of electromagnetic induction to detect changes in magnetic fields. The sensors contain materials with high magnetic susceptibility, due to its good sensibility to external magnetic fields.

In the absence of an external magnetic field, the device is balanced and does not generate output signal. However, when it is oriented along a magnetic field, it becomes unbalanced. This unbalance causes an induced voltage that is directly proportional to the strength of the magnetic field.

To measure the three magnetic field components simultaneously, the triaxial flux-gate magnetometer is used as it has three sensors positioned at right angles to each other that can be aligned with each component of the magnetic field.

In geophysics, this kind of magnetometer is frequently used to measure the Earth's magnetic field and identify its sources and potential magnetic anomalies. They are also used to study the subsurface electrical properties, particularly the conductivity, by measuring the magnetic field in the surface.

III. THE MAGNETOTELLURIC METHOD

The magnetotelluric method (MT) is based on Maxwell's equations. According to Faraday's law, when a primary field penetrating into the Earth encounters a lateral change in conductivity, it induces electric currents which, in turn, according to Ampere's law, generate a secondary field, and the superposition with the primary field is measured at the surface.

The primary field comes from natural geomagnetic sources, like the ionosphere (low frequencies) or lightnings (high frequencies) [4]. For the MT, it can be considered a plane wave propagating vertically into the Earth with a period range from 10^{-5} s to 10^{4} s. In this interval, Maxwell's equations can be simplified by neglecting the displacement current term ($\mathrm{i}\omega\varepsilon\mathrm{E}$) in Ampère's law, in comparison to the conduction current ($\sigma\mathrm{E}$) as $\sigma \gg \omega\varepsilon$, and by assuming that the permeability is equivalent to that in free space ($\mu \approx \mu_0$). Consequently, the characterisation relies solely on the electrical conductivity σ [1].

This study focuses on the relation between the vertical component of the magnetic field variations (H_z) and the horizontal components (H_x, H_y) obtained at a given location and as a function of the frequency.

IV. GEOMAGNETIC TRANSFER FUNCTION

The relation between H_z and H_x, H_y at a given location is known as the geomagnetic transfer function or tipper. In the frequency domain the relation can be approximated as linear:

$$H_z(\omega) = T_x(\omega)H_x(\omega) + T_y(\omega)H_y(\omega), \qquad (1)$$

where T_x and T_y are the North and East components of the tipper vector. It is important to note that these components are complex numbers and that there is a dependence on the frequency. When the tipper value is around 0, it indicates that the subsurface structure is homogeneous or stratified (without lateral variations in electrical conductivity). On the other hand, non-zero values indicate the presence of geological structures with lateral electric conductivity contrast.

The real component of the tipper indicates the direction of the induced currents, and hence lateral conductivity contrast which can be related, for instance, to geological structures. The imaginary component represents the out-of-phase component of H_z relative to H_x, and H_y. Its magnitude provides information on the variations in the medium's electrical properties with depth, as well as other effects such as anisotropy.

Depending on the frequency, information at different depths can be obtained. Short periods (high frequencies) are used to study more superficial structures, whereas long periods (low frequencies) are used to study deeper structures.

V. INSTRUMENTATION

For the experiment conducted in this work, two measuring stations have been used: the Lemi, and the Bartington. It is important to know some of the characteristics of the instruments that compose each station, as well as the applications recommended by each manufacturer.

The LEMI-417 is designed for deep sounding of the Earth's crust and the determination of vertical resistivity profile parameters down to 400 km. It has 2GB of data space and low energy consumption, allowing autonomous operation for up to 6 months [5].

The Mag-03MC70 is described as a high performance fluxgate sensor that provides precision measurements of static and alternating magnetic fields in three axes. Some of the typical applications are magnetic field monitoring and site surveys prior to MRI or Electron Microscope installation [6].

The DATA-CUBE3 type 2 is ideally suited for field installations to reliably record seismic data. Its low power consumption and 32GB of memory capacity allow long-term passive seismological measurement campaigns. DigOS also provides customized adapters (breakout boxes) to connect the data logger to a variety of sensors. In this study, an adapter is used to connect the Bartington's sensor [7].

As for the characteristics, the following table contains those relevant for this study [5–7] A 3.

	Lemi	**Bartington**
Measuring range (nT)	±65 000	±70 000
Sensor noise ($\mathrm{pT_{rms}}/\sqrt{\mathrm{Hz}}$)	10	6
Bandwidth (Hz)	0.3	$3 \cdot 10^3$
Sample rate (Hz)	4	$50 - 400$
Resolution (nT)	0.01	$6.83 \cdot 10^{-3}$
Gain	1	$1 - 64$

TABLE I: A table gathering the relevant station characteristics for this study.

In this study, the 50 Hz sample rate and no gain options were used for the Bartington, and 4 Hz and no gain for the Lemi. As for the Ebre Observatory, they use a set of LEMI at 1 Hz of sample rate to measure the magnetic field.

VI. DATA ACQUISITION AND PROCESSING

The first step of this study consists in learning to set up the devices, and to extract and convert the recorded data into a readable file. For the set up, one of the horizontal sensors of the flux-gate magnetometer is oriented to East by adjusting the magnetometer orientation until this sensor's reads are near zero. This ensures the alignment of the other horizontal sensor with the main direction of Earth's magnetic field (North). The vertical sensor, then, is aligned using a level, and measures the

vertical variations of the magnetic field.

Prior to fieldwork, a test was conducted in the garden of the Faculty of Biology at the University of Barcelona to confirm the correct operation of each element (connections, cables, sensors, ...) of the stations.

Data acquisition was done in a forest near Rofes, Catalonia, a location relatively far from urbanised and industrial areas, to minimize noise interference. Here, both Lemi and Bartington were set up a few meters apart. The Lemi was partially buried and covered with a a bucket, and the Bartington was buried 3 cm below the surface to prevent the effects of the vibrations and temperature variations. Both recorded magnetic field data for seven and five hours at 4 Hz and 50 Hz, respectively.

For the data analysis, a MATLAB-based program designed for a complete MT processing was provided. This program was used as a reference to write the data-analysis program used in this work. First, it was translated into Python, as it is the programming language I am more familiar with, and then modified to focus only on the magnetic field analysis. The program's new features include multi-file analysis, a filter to remove data from the instrument calibration and error-induced divergences, extraction and incorporation of recording times into temporal axes, and the representation of synchronized time series, the spectrum of the magnetic field and the tipper in vectorial form.

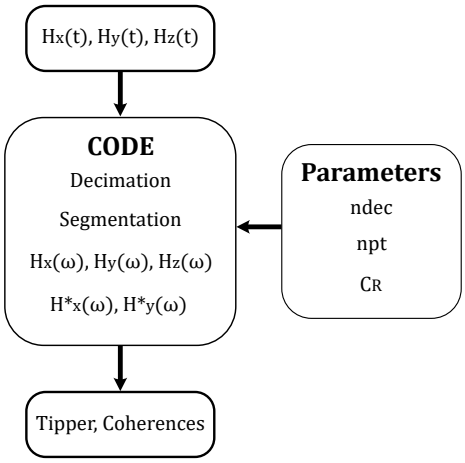

FIG. 1: Diagram of the program used in this study featuring the key points of the process in the CODE panel, and the key parameters in Parameters panel.

The program follows the methods of data analysis found in [8]. It takes as input the magnetic field data from each station. Then the data can be decimated with the **ndec** parameter. This decimation changes the sample rate of the data. To perform a statistical approach the program also segments the data, each segment containing **npt** points. The Fourier transformation and a Parzen filter, defined with the parameter $\mathbf{c_R}$ are then applied. The spectrums and cross-spectrums of the magnetic field are calculated, and, from these values, the program derives the tipper and coherences as outputs. A detailed explanation can be found in B.

For a fair comparison between the Lemi and the Bartington, the sample rate of the Bartigton (50 Hz) is adjusted through the ndec parameter to be the same as the Lemi's (4 Hz). The other two parameters were adjusted through a trial-and-error process, aiming to get the tipper values within the range of (-1, 1) while ensuring smooth tipper and coherence curves as well as small error bars.

In this study, the Batington, Lemi and Ebre ndec is 1, 13 and 1 respectively. The npt and c_r are 16834 and 0.5 for all stations.

VII. RESULTS

This section presents and compares the measured time series obtained in Rofes (Bartington and Lemi), the calculated spectra and the resulting geomagnetic transfer functions. These will be also compared with the results obtained from the time series retrieved from Ebre Observatory (Ebre). Enlarged result figures can be found in D.

Figure 2 shows the recorded magnetic field components as a function of time. For a better visualisation of the behaviour corresponding to each station the data have been detrended. The Bartington and Lemi show a high discrepancy in the behaviour of the magnetic field, with the Bartinton having high frequency and high amplitude variations. When compared to Ebre, the magnetic field of the Lemi is highly similar despite their differing geographical locations.

Figure 3 shows that, for all three directions, the Lemi sensor detects low frequency magnetic signal with big amplitude. The similar behaviour for each component reflects that the three directions measure the same level of noise. The spectra figures of the Bartington (Fig. 9) and Ebre (Fig. 10) show a similar behaviour and can be found in the appendix C.

Figure 4 shows the x and y components of the tipper and the coherences between the magnetic field components H_z with H_x, H_y (coh_z), and H_x with H_y (coh_{xy}) for each station. When comparing the tipper, the three stations show reasonable resemblance. However, the tipper corresponding to the Lemi station has anomalous high values as typical tipper magnitudes are in the range of (-1,1). The error bars of the Bartington and Lemi on the tipper are larger than the Ebre's. As for the coherences, the ones from the Lemi and the Ebre present a similar behaviour, specially coh_{xy}, while the Bartington ones are all near 1. coh_{xy} has similar error bars for the three stations, with those being larger than the coh_z's. The latest are the smallest for the Bartington, followed by the Ebre's and Lemi's, with the Ebre's being a bit smaller.

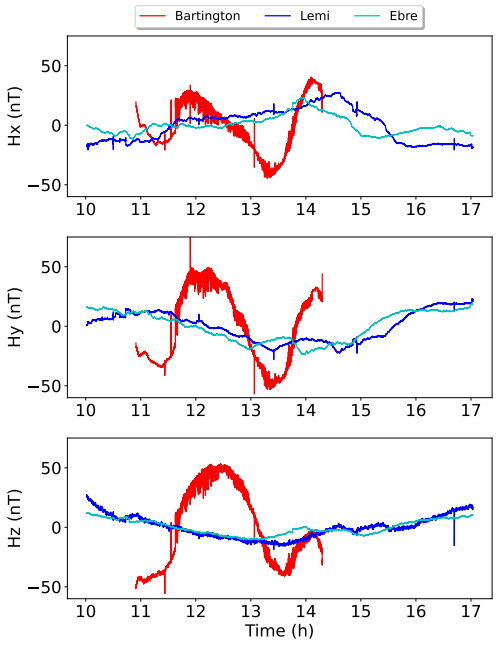

FIG. 2: Time series measurements of the magnetic field for each station. Each panel represents one of the magnetic components as a function of time after detrending the data.

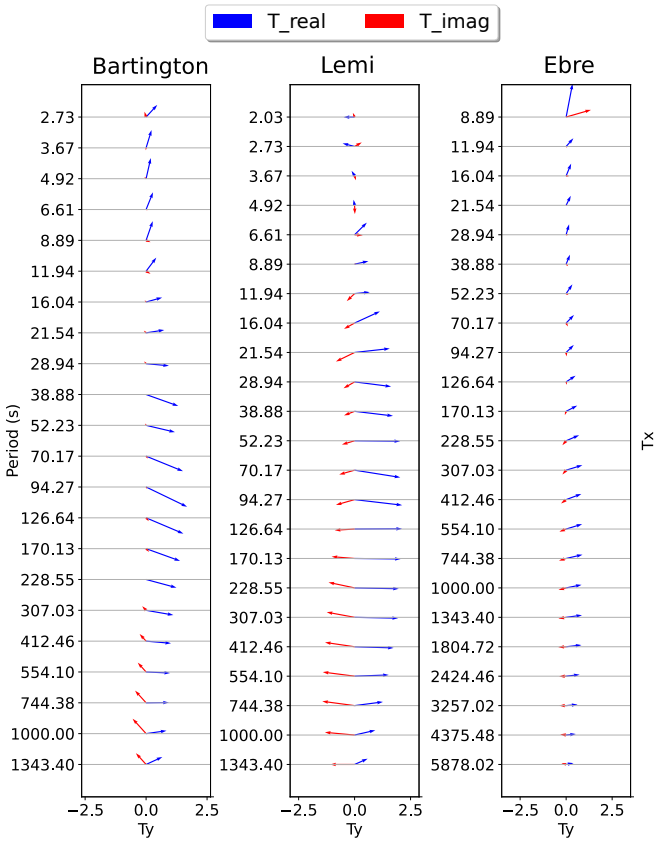

FIG. 5: Variation of the real and imaginary components of the tipper with the logarithm in base 10 of period.

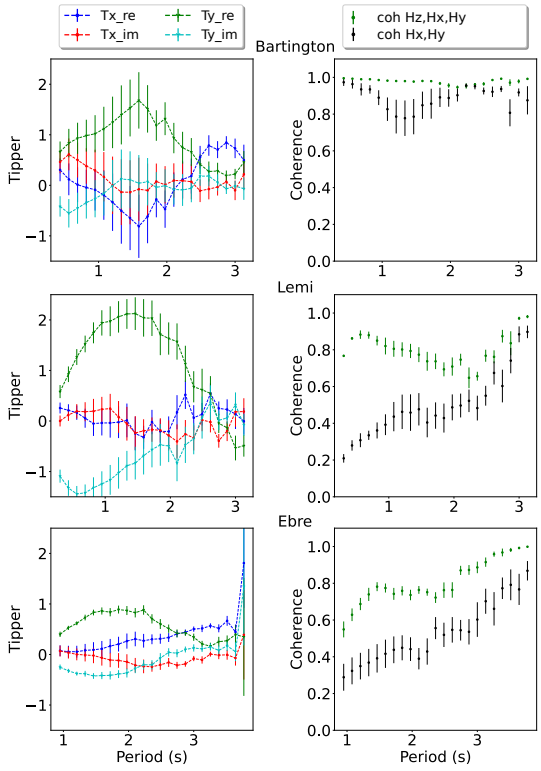

FIG. 4: Variation of the real (re) and imaginary (im) components of T_x and T_y and coherences between H_z and H_x, H_y, and H_x and H_y, as a function of the logarithm in base 10 of the period. Error bars are added.

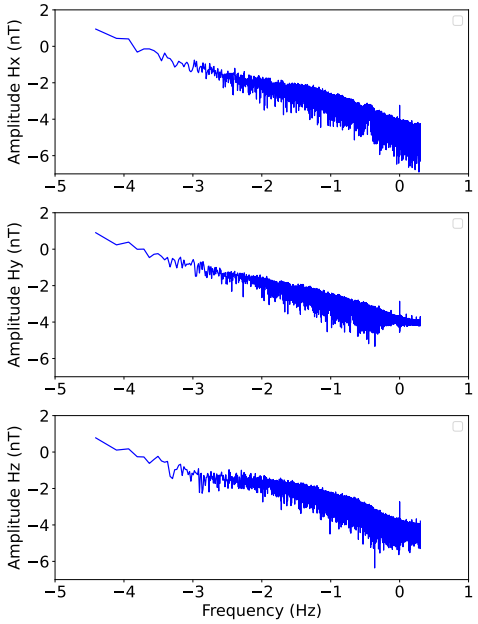

FIG. 3: Normalised amplitude spectrum of the magnetic field measured by the Lemi station. Both axes show the logarithm in base 10 of frequency and amplitude respectively.

The tipper is also represented in vector form (Figure 5) to compare the directions of the real and imaginary vectors for each station. The directions show an almost antiparallel behaviour between the imaginary and real components, which is the typical underground response. There is also some resemblance between measuring stations, with most of the real vectors pointing to the right (East), and the imaginary vectors pointing to the left (West). A general tendency to point more towards north for lower periods (superficial measurements) and slowly point more to the east (real) and west (imaginary) as the period increases (more depth) can be appreciated.

VIII. CONCLUSIONS

The main objective of this work has been achieved. The comparative study has been conducted thanks to the data acquisition experiment and its subsequent analysis using the custom code. From the data acquisition to the results some conclusions can be derived.

- Considering the technical specifications of the Bartington's Mag03-MC70 magnetometer, particularly its high sensitivity, the anomalous variability observed in the magnetic field time series (see Figure 2) could be attributed to the recording of high-frequency ambient magnetic noise. The high tipper values can also be attributed to this reasoning. Nevertheless, the overall results on the tipper and coherences derived from the Bartington data in Figure 4 seem reasonable despite the time series high amplitudes and variability. By taking into account that the tipper and the coherences are relations between the magnetic field components, these results can be explained. If the magnetic field data is equally anomalous for each component, when relating the components it is compensated, and, consequently, tipper and coherence values are the ones expected in this kind of study. The values of the coherence being so close to 1 support this hypothesis. To further prove this point, it is advised to conduct more experiments where the sensor is buried deeper to avoid ambient noise interferences.
- The abnormally high values shown by the Lemi's tipper in the Figure 4, given the resemblance in its behaviour with the other two stations, could be attributed to magnetic ambient noise interfering with the measures. As the Ebre data is also measured using LEMI stations that are well isolated and its tipper values are within the typical range, the abnormal values on Lemi's tipper could be due to not burying the sensor deep enough to ensure its proper isolation. When comparing the coherences, the similarity between the behaviour could be related to the fact that both stations use LEMI instruments.
- As the Bartington and Lemi measured the magnetic field in the same area, both the time-series and TFs should have been the same. This could be attributed to the difference in the station's sensitivity. Given the overall results, the importance of a good installation of the station is evidenced, as most of the abnormalities can be attributed to ambient noise. A further experiment is advised where both stations are properly buried.

- In the light of the accurate magnetic time series from the Lemi shown in Figure 2, and the positive results in tipper and coherences derived from the Bartignton shown in Figure 4, both stations seem to provide complementary data. This suggests the possibility of using both stations to perform complementary subsurface studies.

Acknowledgments

I could not have undertaken this journey without the guidance of Anna Martí Castells and Pilar Queralt Capdevila throughout the study, so I would like to express my gratitude for their knowledge and feedback. Similarly, I extend my sincere thanks to Alex Marcuello Pascual for his help with the code. Additionally, I would like to express my profound gratitude to my partner, and mention my family and my friends, who encouraged me throughout the degree and kept me from giving up.

[1] Rosell Novel, O. (2013). *Caracterització litosfèrica de zones geològicament complexes mitjançant el mètode magnetotel·lúric: casos d'Alberta (Canadà) i de la Serralada Bètica (Espanya)*. Universitat de Barcelona. pp. 1-26.

[2] Ebre Observatory. (2024, April 24). Data of geomagnetic field retrieved on April 24th 2025. Ebre Observatory.

[3] Lawrie, W. (2007). *Fundamentals of Geophysics*. Cambridge University Press.

[4] Campanyà i Lloret, J. (2013). *Innovation of the Magnetotelluric method and its application to the characterization of the Pyrenean lithosphere*. Universitat de Barcelona. pp. 63-82.

[5] Laboratory for ElectroMagnetic Innovation. (2016). LEMI-417M Long-period Magnetotelluric Station. Laboratory for ElectroMagnetic Innovation.

[6] Bartington Instruments. (n.d.). Mag-03 Three-Axis Magnetic Field Sensors. Bartington Instruments.

[7] DigOS Potsdam GmbH. (2021). Datasheet 03-20 DataCube3. DigOS Potsdam GmbH.

[8] Friedrichs, B. (2002). Chapter 3 Methods of Data Analysis. In *PROCMT User's guide* (pp. 61-84). user manual, Metronix.

Mesures del camp geomagnètic: calibració d'instruments i processat

Author: Helena Bermúdez González, hbermugo7@alumnes.ub.edu
Facultat de Física, Universitat de Barcelona, Diagonal 645, 08028 Barcelona, Spain.

Advisor: Anna Martí Castells, annamarti@ub.edu

Resum: En el camp de la geofísica, les variacions temporals del camp electromagnètic s'utilitzen per estudiar tant l'activitat solar com el camp geomagnètic i per caracteritzar les propietats elèctriques del subsol. És important conèixer el rang de funcionament i les limitacions del sensors i els *data loggers* emprats per a la digitalització de les mesures. El processat de les sèries temporals permet calcular les funcions de transferència a partir dels senyals mesurats i convertits al domini de freqüències. L'objectiu d'aquest treball és comparar les series temporals i funcions geomagnètiques obtingudes a partir de dos instruments diferents i amb les obtingudes a partir de les dades de l'Observatori de l'Ebre. Donat que les dades van ser preses a latituds semblants, és raonable fer la comparació. Els resultats mostren similituds i discrepàncies tant en la comparació de les sèries temporals com en la de les funcions de transferència. A més, cap dels dos instruments destaca respecte l'altre en el conjunt dels resultats.
Paraules clau: Camp geomagnètic, equacions de Maxwell, tipper, anàlisi temporal, mètode magnetotel·lúric.
ODSs: Aquest TFG està relacionat amb els Objectius de Desenvolupament Sostenible (SDGs) 7 and 9.

Objectius de Desenvolupament Sostenible (ODSs o SDGs)

1. Fi de la es desigualtats		10. Reducció de les desigualtats	
2. Fam zero		11. Ciutats i comunitats sostenibles	
3. Salut i benestar		12. Consum i producció responsables	
4. Educació de qualitat		13. Acció climàtica	
5. Igualtat de gènere		14. Vida submarina	
6. Aigua neta i sanejament		15. Vida terrestre	
7. Energia neta i sostenible	X	16. Pau, justícia i institucions sòlides	
8. Treball digne i creixement econòmic		17. Aliança pels objectius	
9. Indústria, innovació, infraestructures	X		

El contingut d'aquest TFG, part d'un grau universitari de Física, es relaciona, principalment, amb l'ODS 7, concretament amb les fites 7.2 i 7b, donat que l'estudi del subsol pot ajudar en l'exploració de recursos geotèrmics i energies renovables. També es pot realcionar amb l'ODS 9, fita 9.4, ja que aquest treball està enfocat en la comparació i calibració d'instruments de mesura del camp de la geofísica amb l'objectiu d'estudiar les tecnologies de mesura i la seva eficiència en la presa de dades.

Appendix A: OPERATION OF THE BARTINGTON STATION

1. Solving the discordance between the output of the sensor and the input of the data logger

The Bartington measuring station consisting con the Mag03-MC70 magnetometer and the Data-Cube3 data logger counts with a BoB adapter, from DigOS, to ensure the correct functioning of the station.

From the data sheet from both instruments, the sensor and the data logger, we have the following information:

CUBE:
Full scale input: 4.096 V.
Resolution: 24 Bit per channel.

MAG03-MC70:
Measuring range: ± 70 μT (± 10 V).
Scaling: 143 mV/μT.

On the basis of these instrumental properties a problem arises. The output voltage of the sensor is ± 10 V whereas the input accepted by the data logger is ± 2.048 V, leading to a systematic saturation of the data if both instruments are connected directly.

To address this problem, an adapter (Breakout box, referred as BoB) is implemented in between. This adapter divides the output from the sensor by four. This way, the output range is ± 2.5 V, which is closer to the range of the data logger's input.

Given that the typical values of the geomagnetic field at the latitudes in which the experiment is conducted doesn't surpass the 30 μT, the typical output values will not surpass ± 1.073 V. This way the problem regarding the incompatible output and input ranges is solved.

2. Conversion of the output data to nanoteslas

The recorded data with the Data-Cube is written in bits, instead of nanoteslas, so, when processing the data, a conversion is required.

To do so, we'll use the relation between bits and voltage provided by the data-cube sheet and the relation between voltage and nanoteslas found in the Mag03-MC70 specifications.

Knowing 4.096 V correspond with 2^{24} bits, it's easy to derive that 1 mV are equivalent to 2^{12} bits.

With the scaling specified for the sensor, the relation between voltage and nanoteslas is directly found, being 0.143 mV to 1 nT.

Before computing the conversion, it is important to remember the adapter implemented, dividing the output from the sensor by four.

Now it is easy to find the relation between bits and nanoteslas using the voltage:

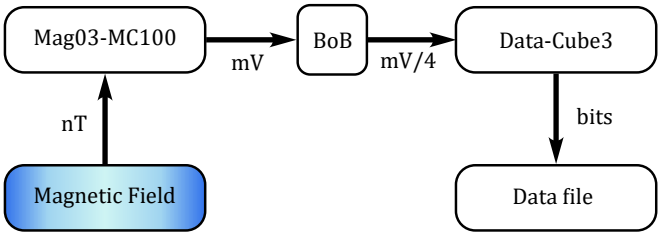

FIG. 4: Visual summary of the Bartington station operation.

$$1 \text{ nT} = \frac{2^{12} \text{ bits}}{1 \text{ mV}} \frac{0.143 \text{ mV}}{4} = 146.432 \text{ bits}. \quad \text{(A1)}$$

When doing the data analysis, the output file data from the Bartington station is divided by 146.432. This way, the data will be in nanoteslas and ready for its analysis.

3. Computing the station resolution

The Bartington station consists on a sensor and a separated data logger. Its sensibility depends on both the instrument and data logger resolution. In this case, the data logger resolution is significantly lower than that of the sensor, so the resolution of the station is dictated by the data logger.

The data logger resolution is provided in bits, but knowing the relation between bits and nanoteslas derived in A 2 (Eq. A1)the resolution in nanoteslas can be computed:

$$\text{Resolution } = 1 \text{ bit} \frac{1 \text{ nT}}{146.432 \text{ bits}} = 6.82910^{-3} \text{ nT}. \quad \text{(A2)}$$

Appendix B: DESCRIPTION OF THE PROGRAM OPERATION

A program for data analysis was written in Python to analyse the magnetic field data measured by each station. The analysis includes the representation of the magnetic field time series, and its spectrum. It also calculates the tipper and the magnetic field coherences through and plots them in function of the period.

The program only accepts text file extensions, so the data file exported from each data logger needs to be converted into a readable text file before the analysis. The Lemi data logger comes with a program that, among other functionalities, converts the data file into a text file. As for the Cube, a set of Java Runtime Environmat (JRE) commands are provided. Among these commands, there's a subset aimed for the conversion of the data file to different formats.

The code reads the text files and stores the data registered for every component of the magnetic field and the start time of the recording. The data can be decimated,

if desired, by giving a value to the **ndec** parameter, with 1 being the value for no decimation. The sample rate of each data logger needs to be specified taking in to account the decimation.

It is important to remember that de data from the Cube data logger is written in bits, so a conversion to nanoteslas using the relation derived in A 2 is done before proceeding with the analysis.

If the instrument was recording while its calibration, a few minutes of data are invalid for the analysis and needs to be filtered out, as well as for any data points clearly caused by instrumental error.

With the sample rate and the filtered magnetic field data, the program represents the time series for each station, being the y-axis the magnetic field in nanoteslas and the x-axis the time of the day in hours (Figs. 9,3, 10). A final time series is plotted where the detrended data is represented in the same figure (Fig. 2).

The spectrum of every component of the magnetic field for each station is also represented (Figs. 3, 9, 10). For that, the data is transformed to the frequency domain applying the Fourier's transformation. The y-axis of the figure is the logarithm in base 10 of the amplitude of the magnetic field in nanoteslas, and the x-axis is the logarithm in base 10 of the frequency.

The code, then segments the data sample to do a statistical study of the measurement if desired. By specifying a value to **npt**, one can choose the number of points per segment. If all the data points are given to npt, the program won't perform the statistical study, and no error bars will show in the figures.

To calculate the tipper, the Fourier transform is employed to transition to the frequency domain.

A set of frequencies, the target frequencies, on which the tipper and coherences will be evaluated, are calculated. The number of target frequencies per logarithmic decade can be selected, 7.8 being the number used in this work. For its calculation, the program takes into account the typical range of frequencies at which the MT study usually operates and chooses the number of frequencies specified that are equally distrubuted along the range in a logarithmic scale.

Before applying the Fourier transformation to each segment, a smoothing window (Hanning window) is applied to prevent discontinuities at the boundaries of each segment and the subsequent issues that can arise in the Fourier's transform. A data detrend is also performed to avoid the possible tendencies to show in the spectrum data.

The smoothed and detrended magnetic field data contained in each segment is then transformed to the frequency domain using Fourier transformation. To enhance the quality of the data, a Parzen filter is applied. This filter performs the weighted mean of the data that fall within a bandwidth around the target frequencies. The bandwidth is defined by a radius that can be specified by the user giving values to the parameter $\mathbf{c_R}$.

In the frequency domain, the relation between the vertical component of the magnetic field and the horizontal components is linear (1). As there is a single equation to solve a problem of two unknown variables (T_x and T_y), the equation is multiplied by the conjugate of H_x, H_x^*, to obtain a new equation, and by the conjugate of H_y, H_y^*, to obtain a second equation. This way, the following equations are solved for T_x and T_y:

$$\begin{aligned} H_z \cdot H_x^* &= T_x \cdot H_x H_x^* + T_y \cdot H_y H_x^*, \\ H_z \cdot H_y^* &= T_x \cdot H_x H_y^* + T_y \cdot H_y H_y^*. \end{aligned} \tag{B1}$$

The coherences between the vertical and horizontal components of the magnetic field (H_z with H_x and H_y) and between the horizontal components (H_x with H_y) for each frequency are also calculated.

Then the statistical study is performed by calculating the mean of the tipper and coherences derived from every segment. Using these values, a figure is created where the tipper and coherences (dimensionless) are represented as a function of the target periods, in seconds, for each station (Fig. 4). Additionally, the tipper is represented in vector form for each target period, also in seconds.

Appendix C: ADDITIONAL FIGURES

Some additional figures that the program generates but are not presented in the results can be found here. The data on the time series figures (Figs. 6, 7, 8) are not detrended, while the data on the spectra figures (Figs. 9, 10) is detrended.

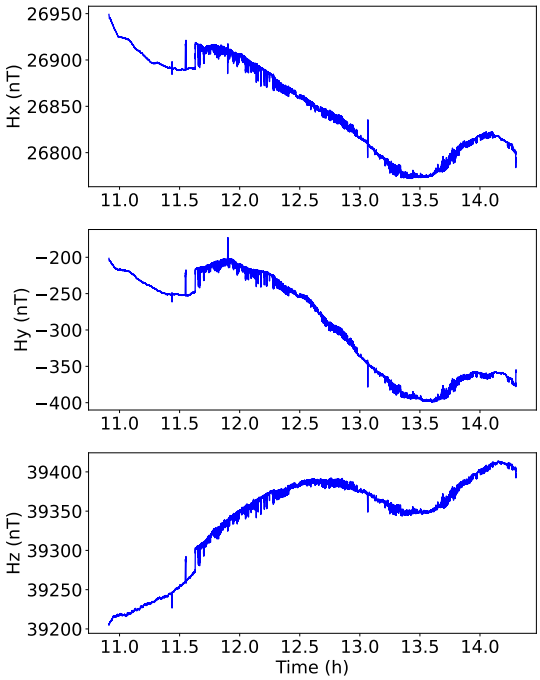

FIG. 6: Time series measurements of the magnetic field for Bartington station. Each panel represents one of the magnetic components as a function of time before detrending the data.

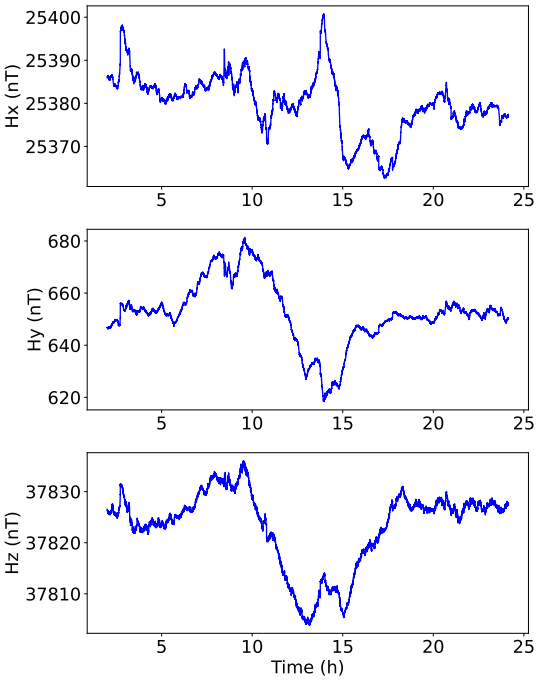

FIG. 8: Time series measurements of the magnetic field for Ebre station. Each panel represents one of the magnetic components as a function of time before detrending the data.

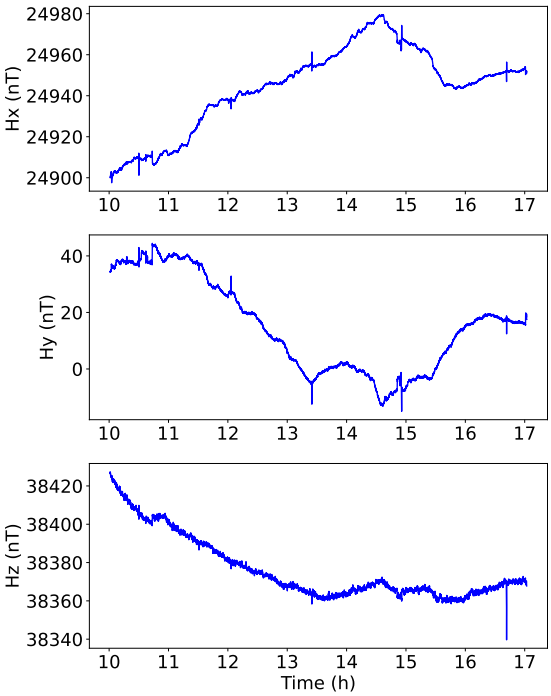

FIG. 7: Time series measurements of the magnetic field for Lemi station. Each panel represents one of the magnetic components as a function of time before detrending the data.

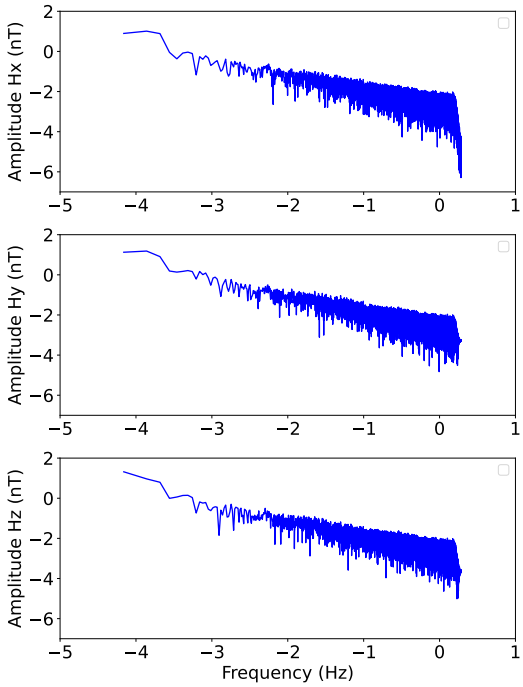

FIG. 9: Normalised amplitude spectrum of the magnetic field measured by the Bartington station. Both axes show the logarithm in base 10 of frequency and amplitude respectively.

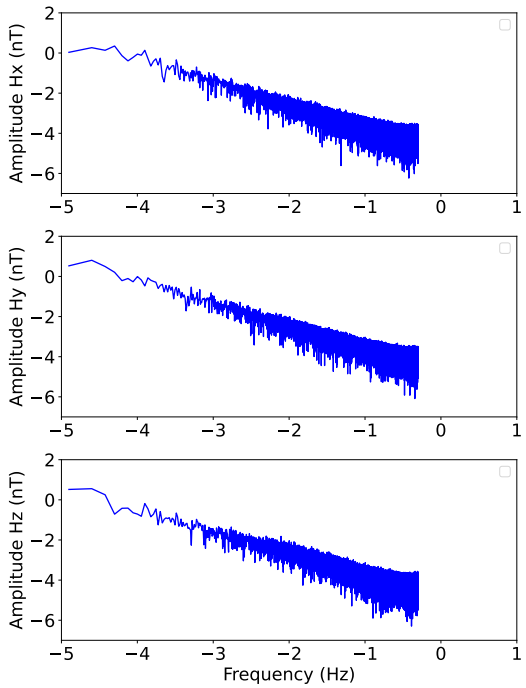

FIG. 10: Normalised amplitude spectrum of the magnetic field measured by the Ebre station. Both axes show the logarithm in base 10 of frequency and amplitude respectively.

Appendix D: ENLARGED RESULT FIGURES

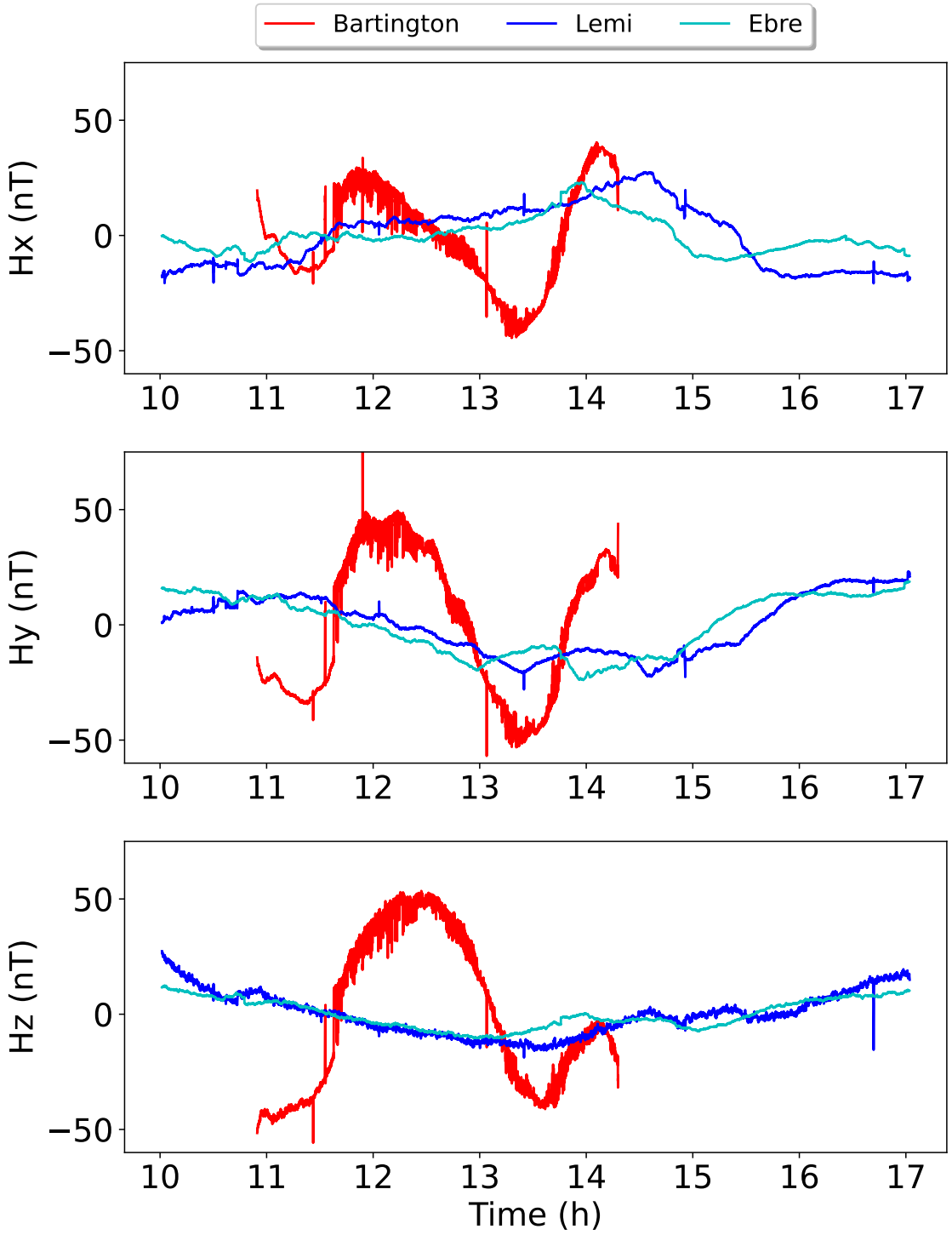

FIG. 11: Larger version of Figure 2.

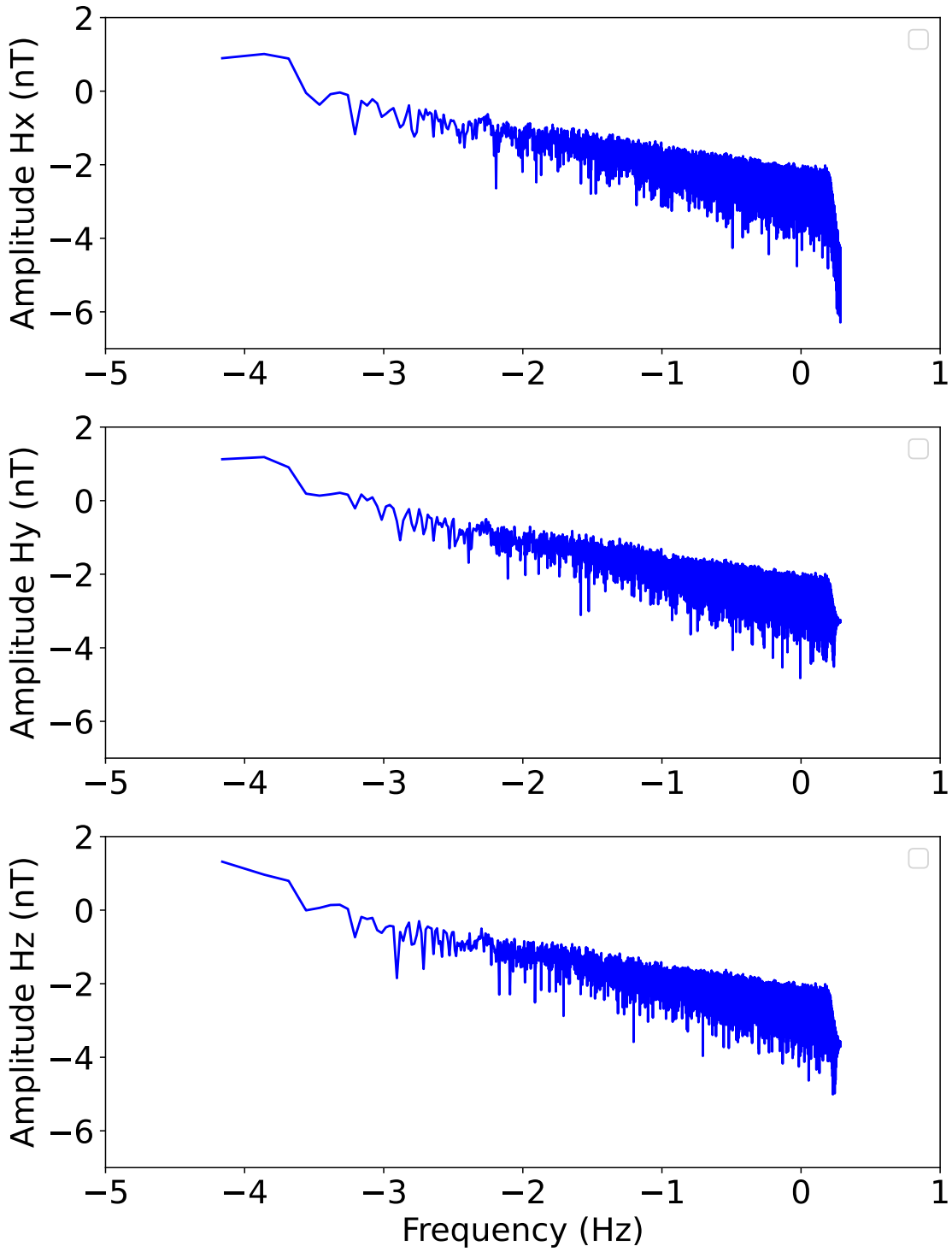

FIG. 12: Larger version of Figure 3.

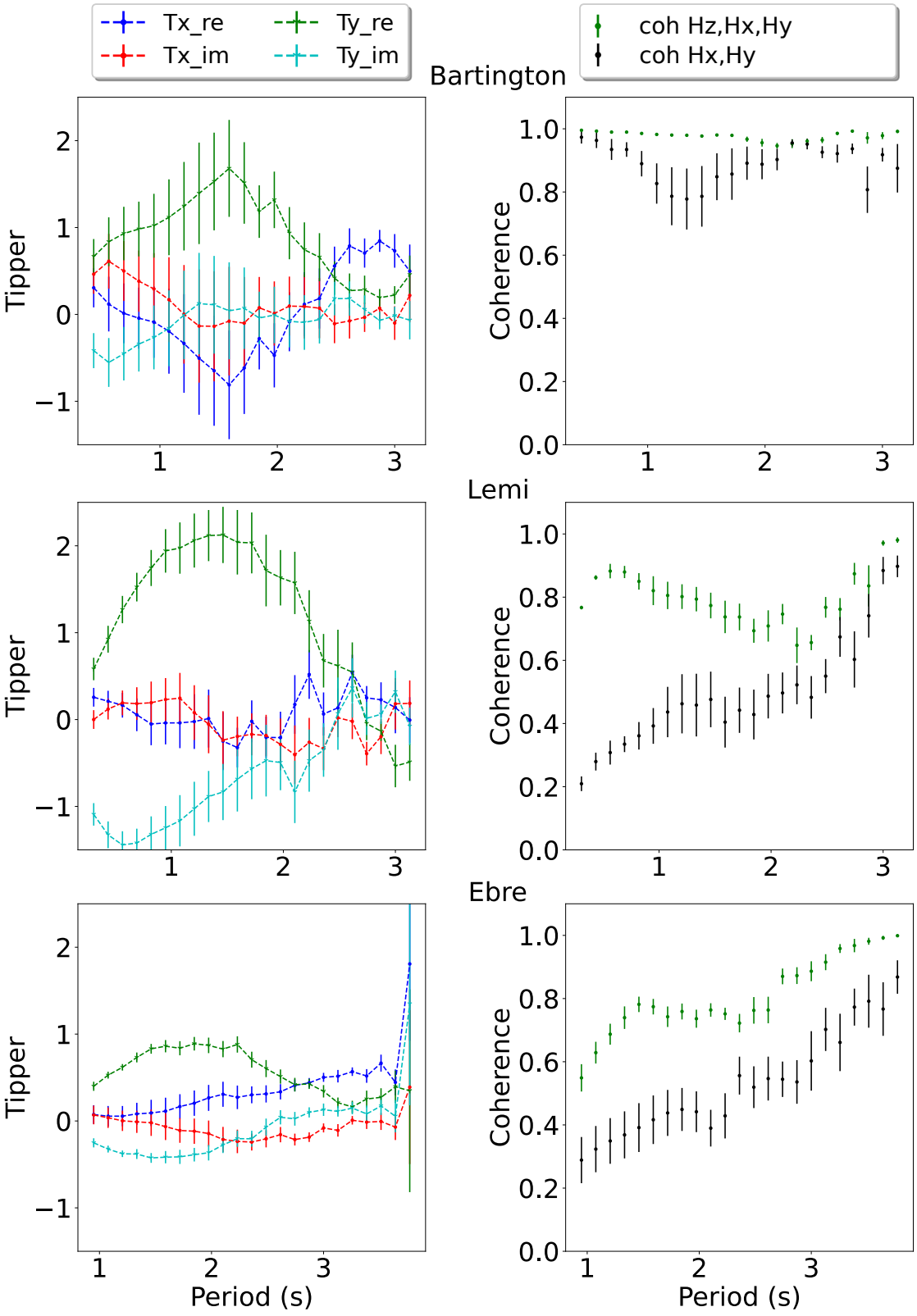

FIG. 13: Larger version of Figure 4.

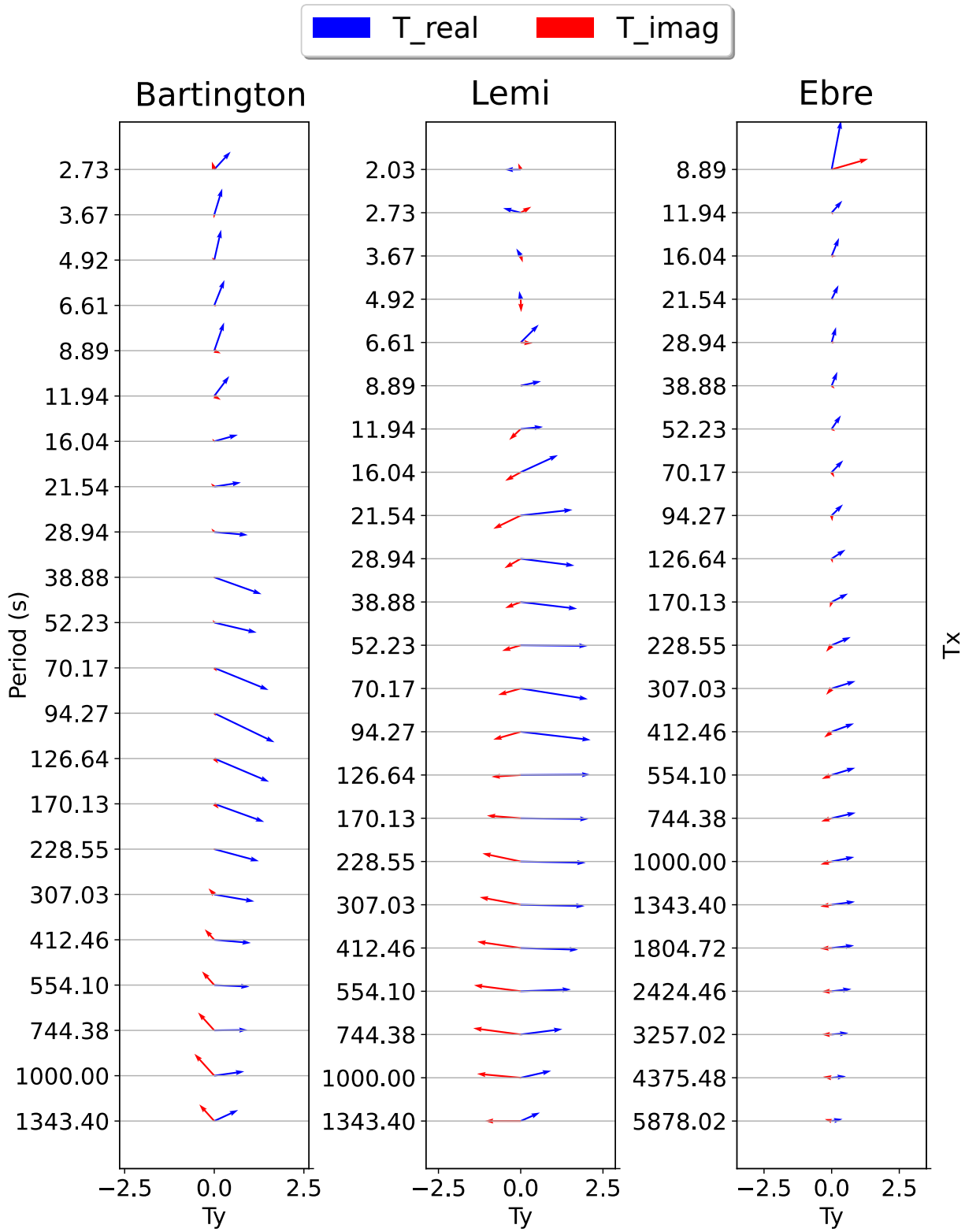

FIG. 14: Larger version of Figure 5.